6ICEGE 6th International Conference on Earthquake Geotechnical Engineering
1-4 November 2015
Christchurch, New Zealand

The 3D Numerical Simulation of Near-Source Ground Motion during the Marsica Earthquake, Central Italy, 100 years later

R. Paolucci[1], L. Evangelista[2], I. Mazzieri[3], E. Schiappapietra[4]

ABSTRACT

In this paper we show 3D physics-based numerical simulations of the devastating Marsica earthquake, Central Italy, occurred 100 years ago. The results provide a realistic estimation of the earthquake ground motion and fit reasonably well both the geodetic measurements of permanent ground settlement, and the observed macroseismic distribution of damage. In addition, these results provide a very useful benchmark to improve the current knowledge of near-source earthquake ground motion, including evaluation of the best distance metric to describe the spatial variability of the peak values of ground motion, as well as the relative importance of fault normal vs fault parallel components.

Introduction

100 years ago, on January 13, 1915, at 6:52 local time, a catastrophic earthquake devastated Marsica, Southern Abruzzi, Central Italy, causing around 33,000 fatalities. Among the most important municipalities hit by the earthquake, the ruin of Avezzano was complete, with 10,700 fatalities, 95% of the total population (CFTI, 2015). A single reinforced concrete building in Avezzano, one of the very first ones at those times, withstood the earthquake and was later declared national monument. Unfortunately, since Italy was about to enter I World War, the government minimized the effects of the earthquake and denied the international support which was a key for the recovery after the Reggio-Messina catastrophe of December 28, 1908, only 4 years before. Therefore, the rescue operations were dramatically slow and some further 3,000 fatalities were estimated because of post-earthquake diseases.

The earthquake was felt up to several hundred km distance: for example, in Rome, about 80 km W of the epicentre, the I_{MCS} intensity was estimated from VI to VII. A sketch of the MCS intensities through the Southern Abruzzi region, together with the surface projection of the fault and the location of the instrumental epicentre is illustrated in Figure 1.

The earthquake was originated by the Fucino fault system (Galadini and Galli, 1999), consisting of an array of NW-SE striking normal faults, dipping mainly SW, which is also attributed to have

[1] Professor, Dept. Civil and Environmental Engineering, Politecnico di Milano, Italy, roberto.paolucci@polimi.it
[2] Researcher, Institute for Coastal Marine Environment (IAMC), National Research Council (CNR), Naples, Italy, lorenza.evangelista@cnr.it
[3] Post-doc researcher, MOX - Laboratory for Modeling and Scientific Computing, Department of Mathematics, Politecnico di Milano, Milan, Italy, ilario.mazzieri@polimi.it
[4] Graduate student, Dept. Civil and Environmental Engineering, Politecnico di Milano, Italy, erika.schiappapietra@mail.polimi.it

generated the earthquake which severely affected Rome in 508 AD (Galli et al., 2012). While clear evidence of the surface fault rupture was pointed out by the post-earthquake survey by Oddone (1915), who followed the fault trace from SE to NW for about 33 km, there is no consensus on the epicentre location. As a matter of fact, this is often reported, such as in CFTI (2015), to be located at the center of the maximum intensity macroseismic area, roughly coinciding with the center of the Fucino basin. In addition, an instrumental determination was proposed by Basili and Valensise (1991), and also reported by Favali and Frugoni (1999) in a special volume dedicated to the Marsica earthquake, based on the available seismometer recordings, which lead to the location 41.975 N – 13.605 E, which has been used in this paper and is shown in Figure 1. Different determinations of the earthquake magnitude are also reported in the literature, and reviewed by Favali and Frugoni (1999), leading to Ms evaluations ranging from 6.6 to 7.0.

The presence of a prevailing normal faulting system bordering a tectonic basin is one of the key features of seismogenic activity in the Central-Southern Apennines, and poses the key problem of coupling the presence of the seismic fault with soft sedimentary basins, having relatively young age and large thickness, thus enhancing the hazard typical of near-source conditions.

In this research, we have simulated near-source ground motion during the Marsica earthquake, taking advantage of the SPEED code, developed at Politecnico di Milano to perform 3D physics-based numerical simulations of seismic wave propagation. These include a kinematic model of the seismogenic fault rupture and a 3D model of the shallow crustal layers, including the complex geological irregularity of the Fucino basin.

Different objectives were pursued during this work, namely: (1) providing hints to constrain the physical parameters of the earthquake; (2) verifying the simulated permanent ground displacements against the vertical settlement of 18 statues, which were placed along the shoreline of the Fucino lake before drainage, and which were used after the earthquake as geodetic benchmarks; (3) verifying possible conditions of directivity and interaction with the soft deposits of the Fucino basin, in order to explain the vast devastation in Avezzano, at the Northern edge of the basin, at some 20 km NW of the epicentre; (4) quantifying some relevant parameters of ground motion in near-source conditions, such as the ratio of strike fault normal (FN) vs fault parallel (FP) components; (5) evaluating the best distance metric to model the peak values of ground motion in near-source conditions.

Geological and Geotechnical Characterization

Geological framework and geotechnical characterization of Fucino basin

The Fucino basin is the most important intra-mountain depression of the Central Apennines, surrounded by high carbonate ridges of Meso-Cenozoic age. It covers an area of 900 km^2, of which 200 km^2 are an ancient lake, drained in 1875. The latter was the last proof of a long geologic evolution started in the Pliocene, during which the area was always lower with respect to the Apennines, interested by uplifting movements. The current geological setting of the Fucino basin, illustrated in the geological map drawn in Figure 2, results from a complex sequence of depositional events, due to erosion and tectonics.

The bedrock consists of Meso-Cenozoic carbonate, generally covered by terrigenous Neogene flysch deposits but also outcropping along the sides of the basin. The bottom of the basin was filled during the Quaternary with continental deposits of variable genesis and deposition age, resulting from lacustrine to subsequent alluvial sedimentations. In detail, the sedimentary sequences were divided (Cavinato et al., 2002) into:

- a Lower Unit (Plio-Pleistocene), outcropping on the North-eastern border of the basin, that mainly consists of breccias and alluvia, with subordinate lacustrine deposits;
- an Upper Unit (Upper Pleistocene-Holocene), made up of interdigitated lacustrine and alluvial deposits, that at the border of the depression heteropically evolves into alluvial fan deposits, which may even be coarse-grained.

Finally, the Quaternary sedimentary sequence is closed by thick lacustrine deposits in the center of the basin (Giraudi, 1999).

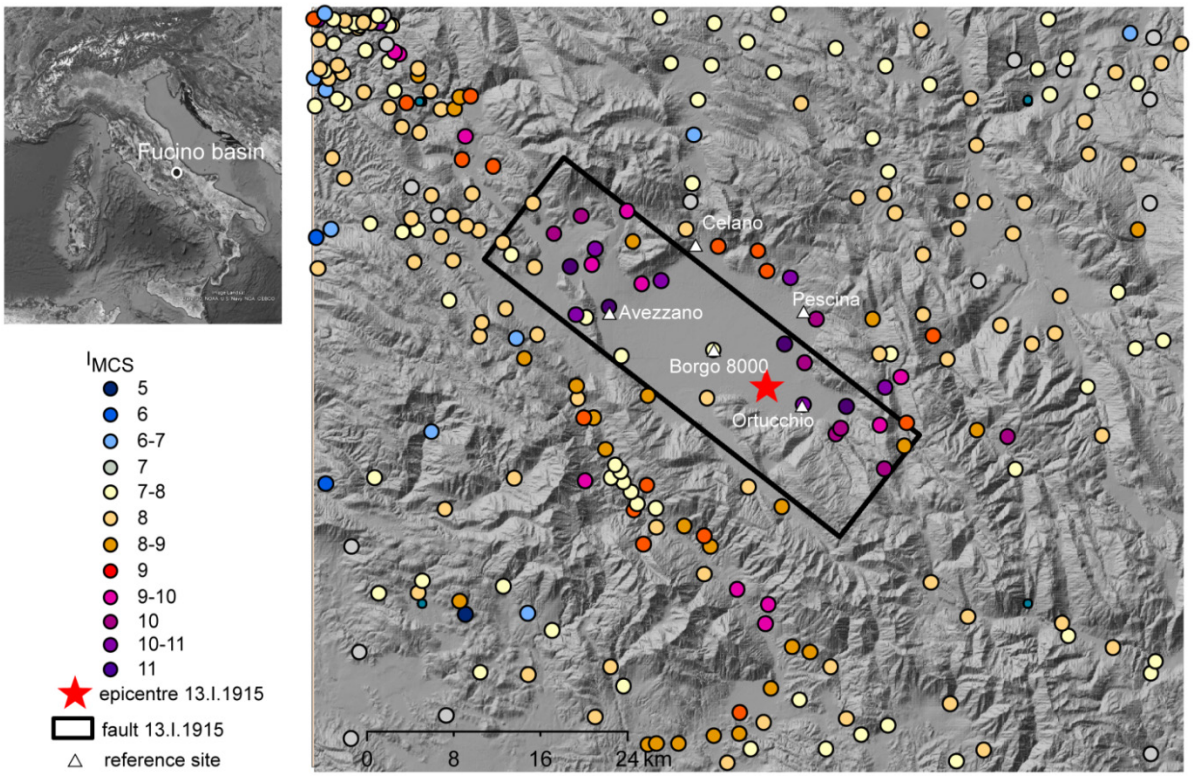

Figure 1. I_{MCS} distribution according to the Italian macroseismic database (emidius.mi.ingv.it/DBMI11/), including the epicenter and the surface projection of the fault adopted in this work.

This geomorphological setting is the result of a post-orogenic relaxing phase of the central part of Apennines, whose normal fault systems, with NW-SE and E-W-trending high-angle and S-SW-dipping, developed extensional basins along the south-western sector of the overthrust belt (Cavinato and De Celles, 1999).

The complex geologic structure is characterized by the overlap, through two separate phases, of two semi-graben; the first one fully developed during the Pliocene, while the second one developed in the Plio-Pleistocene. In Figure 2, the isochron map in two-way time (TWT) of lacustrine deposits from seismic profiles is reported. The map shows the presence of a first sub-basin felt in the North sector near Avezzano with TWT equal to 250 ms and a second well defined depocentre near San Benedetto, the so-called Bacinetto, characterized by TWT of 900 ms.

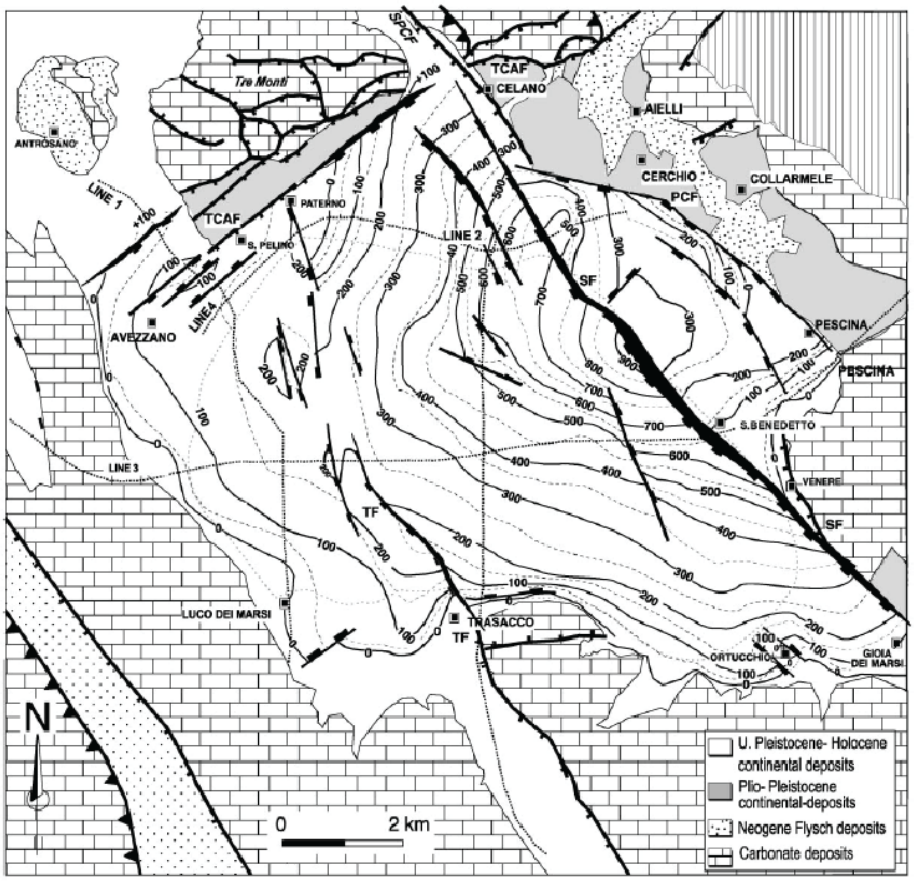

Figure 2. Geological map and isochron contour map (interval 50 ms and 100 ms) of the alluvial and lacustrine deposits (from Cavinato et al. 2002).

The lacustrine deposits, filling the latter sub-basin, was involved by an extensive geotechnical characterization activity in 1986 (Pane and Burghignoli, 1988) to evaluate the dynamic subsoil properties. The specific investigations, planned for the geotechnical characterization, consisted of in situ and laboratory tests: in situ tests included Cross-Hole (CH), Down-Hole (DH) and SASW, while the laboratory program consisted of resonant column (RC) and Torsional Shear (TS) tests. Figure 3a shows the comparison of the in situ shear wave velocity (V_S) profiles. The data from different sources show a good agreement within the investigation depth and a significant increase of V_S with depth. Since the in situ tests investigated only down to the first 40m (Figure 3a), the increase of V_S profile along the whole thickness of lacustrine deposits was described by scaling the law of variation of the small strain shear stiffness (G_0) with the mean

effective stress (p') measured in RC-TS tests (Figure 3a). To this aim, the variation of G_0 with p' observed in the RC-TS tests, was first expressed in terms of shear wave velocity, V_S (white squares in Figure 3a), as a function of depth. This latter was related to p' by assuming a value of the coefficient of earth pressure at rest $k_0 = 0.8$.

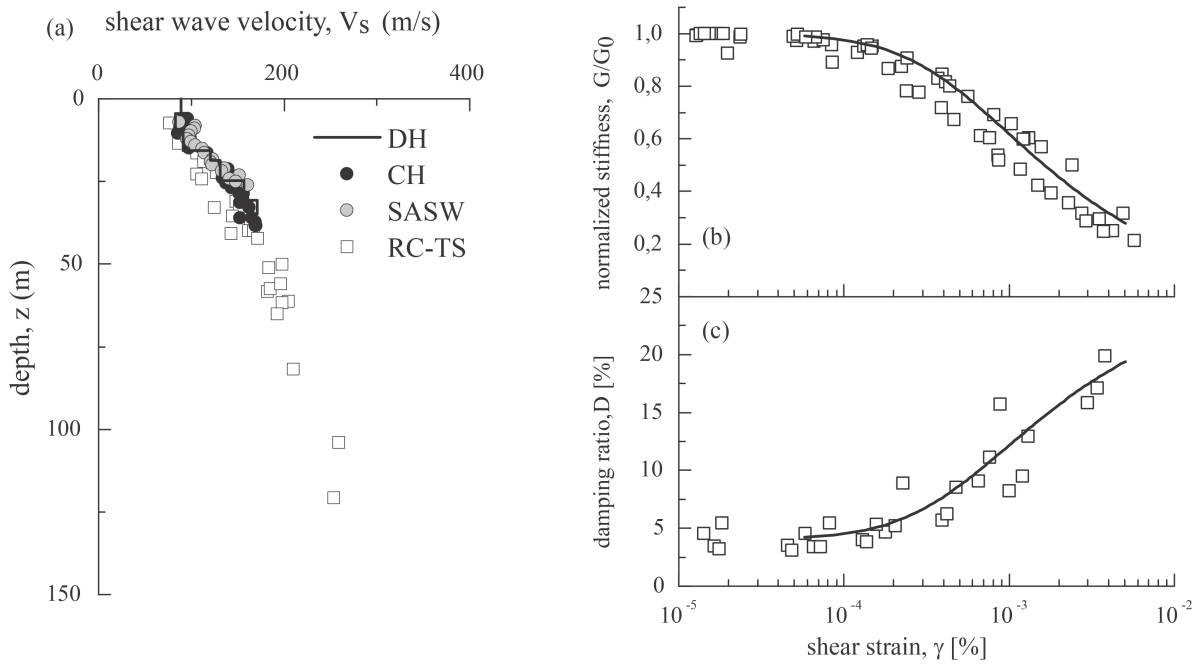

Figure 3. (a) Comparison of shear wave velocity profiles obtained by DH, CH, SASW and RC-TS; Normalised shear modulus (b) and damping ratio (c) versus shear strain from RC-TS tests.

The RC-TS tests confirmed the significant increase of V_S along the thickness of lacustrine deposits and allowed obtaining a shear wave velocity profile down to 100 m.

The non-linear behavior of lacustrine deposits was modeled based on the results of laboratory tests, reported in Figure 3b-3c, in terms of variation of the normalized shear modulus, G/G_0, and the damping ratio, D, with the shear strain, γ. The variation of G/G_0 vs γ is typical of medium-high plasticity clay. The data is then interpolated with the Ramberg-Osgood law. Instead, the variation of damping ratio D (Figure 3c) with shear strain γ instead, was obtained by application of the Masing-modified criteria (Hardin and Drnevich, 1972) to the modeled decay curve.

Construction of a numerical model

The numerical model of the Fucino basin extends over an area of 56x46x20 km^3 (Figure 4). It is built by glueing the topographic layer, obtained by a 250 m Digital Elevation Model, with the underlying layers describing the bedrock morphology as provided by seismic profiles (Cavinato et al., 2002). The fault geometry is also included into the model, as it will be discussed in the following section.

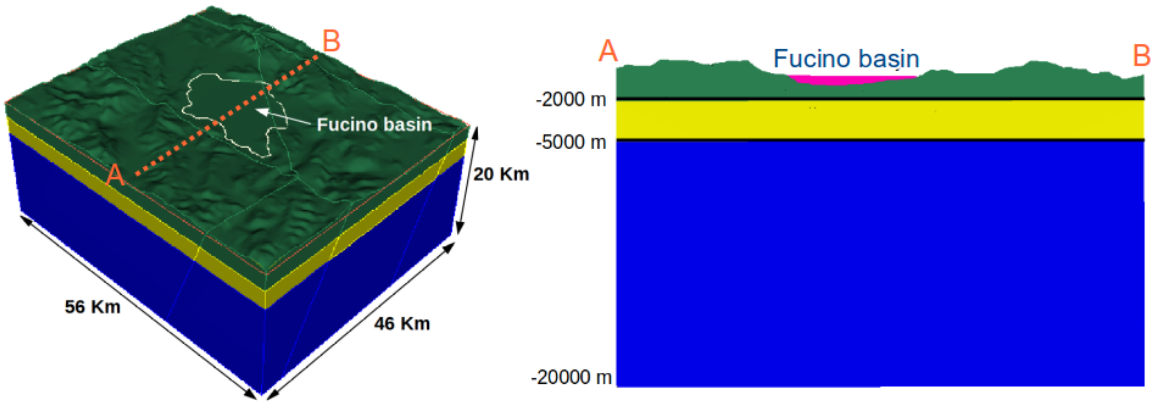

Figure 4. 3D numerical domain, with a representative cross-section, transverse to the Apennine chain.

The bedrock morphology is derived by the interpretation of seismic profiles shown in Figure 2. In fact, assuming the P-wave velocity for bedrock V_P = 2000 m/s (Cara et al, 2011), it is possible to derive the depth of the basin; in particular the first sub-basin near Avezzano reaches a depth of 250 m, while the deeper one, corresponding to the Bacinetto, is characterized by a maximum depth of 900m.

According to the geotechnical characterization, the filling deposits are assumed to behave as a non-linear visco-elastic medium, characterized by a unique profile of density (ρ), Poisson ratio (ν) and shear wave velocity (V_S). The latter is the result of the joint interpretation of in situ and laboratory tests to obtain a reliable geotechnical modeling of the subsoil. All the V_S data are fit with a power function and finally scaled to best approximate the in situ values in order to deduce the profile down to the bedrock depth.

The estimated model of V_S is in good agreement with those derived by Cara et al. (2011) from experimental measurement of resonance frequency by standard spectral ratio (SSR) and horizontal-vertical spectra ratio (HVSR) methods.

The quality factor Q is derived directly by the V_S values and is assumed to be proportional to frequency as $Q = Q_0 f$, with Q_0 set for the target value $Q = V_S/10$, specified at f =0.5 Hz. Then, we can summarize the soil model parameters as follows:

$$\rho = 1530 \cdot 0.1 \cdot z^{0.54} \ \text{(kg/m}^3\text{)} \quad (1)$$

$$V_S = 180 + 10 \cdot z^{0.6} \ \text{and} \ V_P = \sqrt{10} \cdot V_S \ \text{(m/s)} \quad (2)$$

$$Q = V_s / 10 \quad (3)$$

It is worth highlighting that an outcropping bedrock is assumed outside the boundaries of the Fucino basin. Therefore, no detailed result have been obtained to quantify ground motion in valleys outside the Fucino basin, such as Valle del Liri, SW of the basin, which was also badly affected by the earthquake.

A crustal model is adopted based on what suggested by Ameri et al. (2012). It is characterized by five horizontal and parallel layers resting on a half-space at a depth of 20 km. In particular the V_S values of the shallow layers have been reduced with respect to the ones proposed by Ameri et al (2012), in agreement with the site investigations (Working Group AQ-MS, 2010) in order to attenuate the impedance ratio at the bedrock. The properties of each layer are shown in Table 1.

Table 1 Horizontally stratified crustal model assumed for the 3D numerical simulations.

H (m)	V_S (m/s)	V_P (m)	ρ (kg/m^3)	Q
500	1000	1800	2300	100
1000	1700	3160	2500	150
2000	2600	4830	2840	250
5000	3100	5760	2940	300
20000	3500	6510	3180	350

Kinematic modeling of the seismic source

There is a general consensus that the Marsica earthquake was generated along the Fucino system of normal faults (Galli et al., 2012), which borders on the Eastern side the Fucino basin, the strike of which is aligned along the Apennines chain. This indication is well constrained by the post-earthquake survey of Oddone (1915), who clearly witnessed the evidence of the line formed by the surface fault rupture, extending about 30 km from SE to NW, by the downward settlements of the geodetic benchmarks placed around the Fucino lake before drainage in 1875, on the hanging wall side of the rupture (Ward and Valensise, 1989; Berardi et al., 1995; Amoruso et al., 1998), and by the numerous paleoseismological studies in that area (Galadini et al., 1997; Galadini and Galli, 1999; Galli et al., 2012).

The set of fault parameters considered in our numerical simulations is summarized in Table 2, while the slip distribution is illustrated in Figure 5. We based the geometric parameters (dimensions, position, strike, dip, rake) on Galadini (personal communication, 2015), the slip distribution on Ward and Valensise (1989), and the epicentre on the instrumental location by Basili and Valensise (1991). By modulating the amplitude of slip distribution, we considered a range of M_W from 6.7 to 7. The value M_W 6.7 reported in Table 2 is the one for which the best agreement was obtained with the benchmark settlements, as shown in Figure 6.

Numerical modeling of seismic wave propagation by Spectral Elements

SPEED: Spectral Elements in Elastodynamics with Discontinuous Galerkin

The numerical open-source software SPEED (http://speed.mox.polimi.it) is designed for the simulation of elastic wave propagation in complex geological configurations. The code is jointly developed at the Department of Mathematics and the Department of Civil and Environmental Engineering of Politecnico di Milano. The SPEED kernel is based on a discontinuous version of the classical Spectral Element (SE) method and early applications to computational seismology can be found, for instance, in Faccioli et al. 1997; Komatitsch and Tromp 1999; Seriani et al. 1995. Based on the work of Antonietti et al. (2012), to better exploit the hp-nature of spectral elements the SE formulation has been extended to address discontinuous approximations.

Table 2. Fault parameters adopted in this work.

Fault Parameters	Present study
Fault Origin F_O (Lat, Lon)	(42.15, 13.37)
Top Depth of Fault H_{min} (km)	0.337
Length along Strike L (km)	41.6
Width along Dip W (km)	20
Epicenter (Lat, Lon)	(41.97, 13.60)
Focal Depth (km)	6.4
Strike (°)	127.8
Dip (°)	53.3
Seismic moment M_0 (Nm)	$1.25\ 10^{19}$
Mw	6.7
Rise time τ (s)	0.70
Rupture Velocity V_R (m/s)	0.85 V_S
Rake (°)	260

Fault Geometry

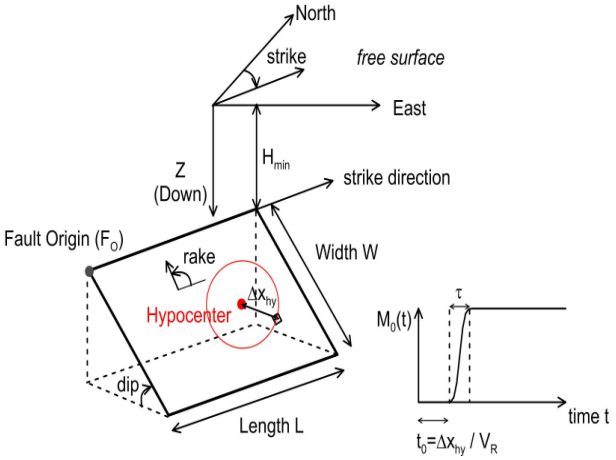

Discontinuous Galerkin Spectral Element (DGSE) approaches are shown to be able to capture local variations of the physical solutions while locally preserving the same accuracy of SE methods in term of dissipation and dispersion errors. DGSE methods can handle non-matching grids and different local approximation degrees making such schemes much flexible than SE approaches (at price of an increased computational complexity). Furthermore, DGSE methods enjoy a high level of intrinsic parallelism, making such a discretization technique well suited for massively parallel computations (Paolucci et al. 2014).

The present version of SPEED includes the possibility to treat linear and non-linear visco-elasticsoil seismic wave propagation in heterogeneous media, either with frequency proportional quality factor (Stupazzini et al. 2009), or frequency constant quality factor (Moczo et al. 2014). Paraxial boundary conditions (Stacey 1988) are introduced to reduce spurious reflections from outgoing waves inside the computational domain, while time integration can be performed either by the second order accurate explicit leap-frog scheme or the fourth order accurate explicit Runge-Kutta scheme (see Butcher 2008).

Recently, SPEED has been successfully applied for the numerical simulation of near-source ground motion during the 2012 Po plain seismic sequence in Italy (Paolucci et al., 2015), for hazard assessment analysis in large urban areas for reinsurance evaluations as described in Paolucci et al. (2014), as well as for city-site interaction problems related to the dynamic response of complex infrastructures (Mazzieri et al. 2013) where the multi-scale phenomena should be taken into account in the same model.

Spectral Element model and numerical performance

The computation domain used for the numerical simulations has been built based on the model described in Section 2.2. Considering a rule of thumb of 5 grid points per minimum wavelength for non-dispersive wave propagation in heterogeneous media by the SE approach (cf. Antonietti et al. 2012), and considering a maximum frequency f_{max} = 2 Hz, the model consists of 156.562 hexahedral elements, resulting in 10.185.545 degrees of freedom, using a fourth order polynomial approximation degree.

In particular a conforming mesh consisting has been set up having size varying from a minimum of 200 m, within the quaternary basin, up to 440 m in the outcropping bedrock, and reaching 1250 m in the underlying layers, see Figure 5 (left). The source time history is given by an approximate Heaviside function, as follows:

(4)

where M_0 is the scalar seismic moment, erf $(\cdot)$ is the error function and τ = 0.7 s is rise time. To enhance the high-frequency radiation, a random variability of rise time and rake angle around their average value is considered, with self-similar spatial correlation (Smerzini and Villani, 2012). Moreover, to avoid the onset of very high velocity pulses due to super-shear effects, the rupture velocity has been bounded to $V_R = 0.85V_S$, being V_S the shear wave velocity at the corresponding source depth.

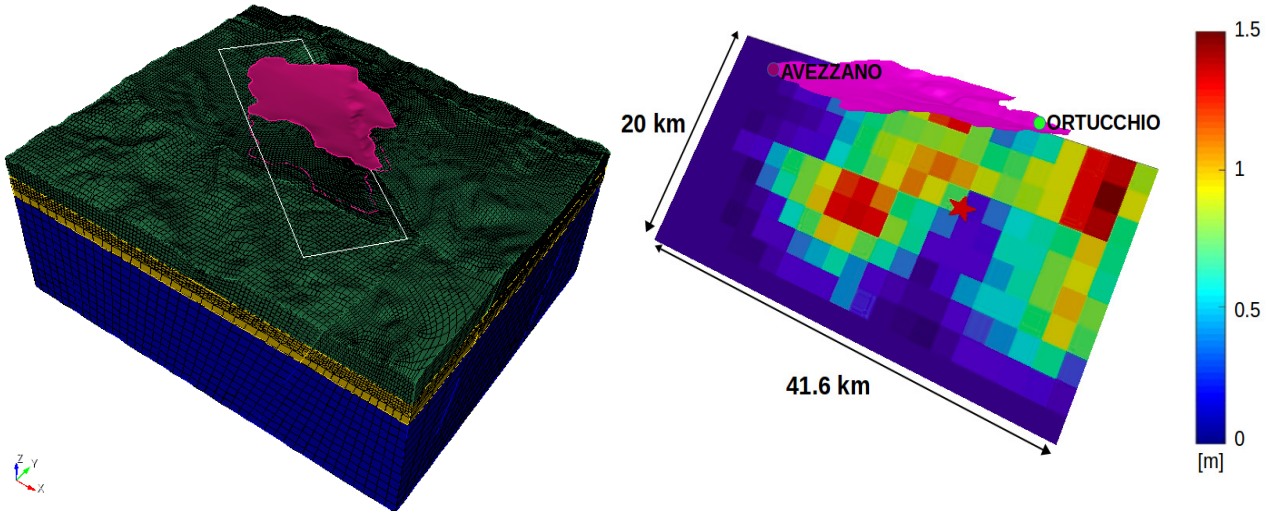

Figure 5. (Left) 3D computational mesh adopted for the numerical model along with the projection of the seismic fault responsible of the January 13 1915 earthquake and buried topography, corresponding to Quaternary sediments in Figure 2. (Right) Assumed slip distribution to model the earthquake fault rupture, as described in Section 3.

The 3D seismic velocity model has been derived in the basis of the geological data described in Section 2 (see equations (1-3) and Table 2). It should be remarked that the resulting 3D numerical model is a compromise between, on one side, the need to fit as closely as possible the available geological and geophysical information throughout a large spatial region, and, on the other side, to cast such information within a reasonably simple form apt to construct the computational model.

The distinctive features of the numerical model are (i) a kinematic representation for the seismic fault rupture of the 13 January 1915 earthquake, see Figure 5 (right), and (ii) inclusion of a 3D velocity model of the Fucino valley, taking into account the spatial variation of the most relevant geologic discontinuities beneath the surface sediments, which have significant effects on the seismic wave propagation, see Table 2 in Section 3.

For the numerical simulations the time integration has been carried out with the explicit second order accurate leap-frog scheme, choosing a time step equal to 0.001 s for a total observation time T = 50 s. The simulations have been carried at the Idra cluster located at MOX-Laboratory for Modeling and Scientific Computing, Department of Mathematics, Politecnico di Milano (http://hpc.mox.polimi.it/hardware/) using 32 parallel CPUs, resulting in a total computation time of about 24 hours for a single simulation.

Discussion of results

We have first verified the adequacy of the fault slip distribution model by comparing the simulated vertical displacements with the post-earthquake geodetic measurements (Loperfido, 1919, values taken from Berardi et al., 1995). The comparison is shown in Figure 6 (right side) for two values of M_W, obtained by changing the amplitude of slip distribution. The best agreement was found for M_W 6.7, compatible with the best solution of Amoruso et al. (1998) who found the minimum misfit with M_W 6.6±0.1. As reported by Amoruso et al. (1998), Loperfido (1919) himself underlined that some measurements might have been inaccurate, as benchmark 6, which was pulled off by the earthquake, and benchmark 11, lying on marshland and possibly subjected to additional ground settlements. On the left side of Figure 6, the map of permanent vertical ground displacements is reported, together with the location of geodetic benchmarks. It should be pointed out that the numerical code is based on the assumption of elastic material behavior, so that it cannot model the sharp offset due to the fault rupture. Rather, a regular transition from negative to positive values of displacement is obtained, with very large, albeit elastic, ground strains.

In Figure 7, snapshots of horizontal ground velocity, rotated in the strike fault normal (FN) and fault parallel (FP) components, are shown. The amplification of motion due to basin effects is very clear. Also, it is worth to remark that, while in the initial phase of motion the FN component is prevailing, as it should be due to the normal faulting assumption (although a very small strike slip component is present, as shown by rake angle = 260°, see Table 2), the FP component becomes very clear inside the basin at about 7 s. This is mainly associated to Rayleigh waves, generated inside the basin, propagating in the NW direction towards Avezzano.

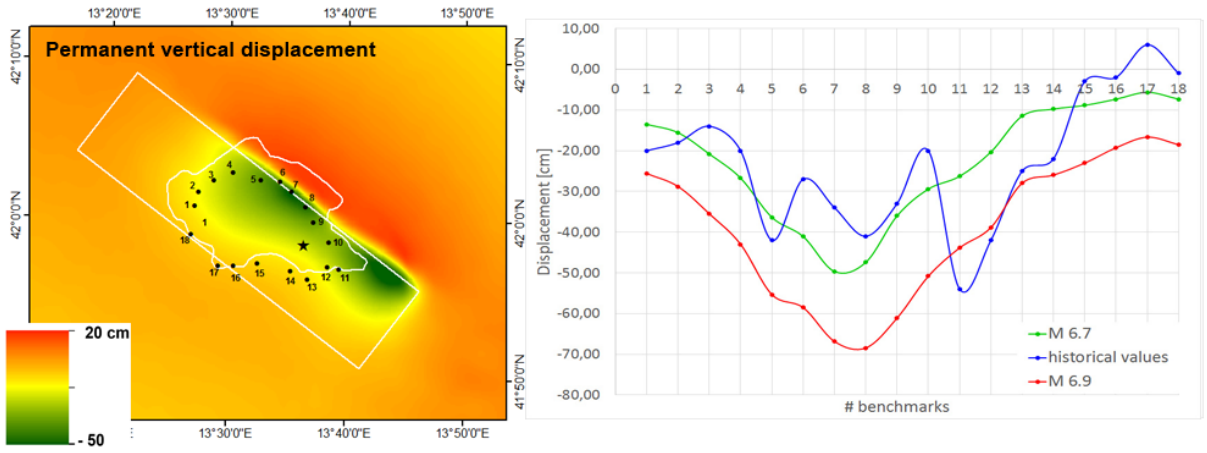

Figure 6. (Left) Map of permanent vertical displacements computed by SPEED for a simulated earthquake magnitude Mw 6.7, with the slip distribution in Figure 5. (Right) Comparison, for different magnitudes, with historical values from geodetic measurements (Loperfido, 1919).

The peak ground velocity (PGV) map of the FN component, together with the corresponding velocity records, is illustrated in Figure 8. Here, the observed variability of ground motion is striking, with the different features of ground motion observed on the footwall (Pescina and Celano) and on the hanging wall of the fault (Ortucchio, Borgo8000, Avezzano) that are probably related to the coupling of different soil conditions and different location with respect to the fault plane. It is also worth to remark that the largest PGV values occur close to the edge of the surface projection of the fault plane. Whether these may be considered as reliable values will be the subject of future research, because in our numerical simulations the energy dissipation due to the surface fault rupture is not accounted for, although a moderate nonlinear response is considered through a nonlinear elastic model following the curves in Figure 3. However, to underline the difficulty in predicting peak ground motion values in the proximity of the fault, it is worth to remark that the available records during the M_W 6.7 Fukushima Amadori, Japan, normal faulting earthquake on April 12, 2011 (Anderson et al., 2013), therefore in similar conditions as the one under study, have shown PGV values larger by a factor ranging from 1.4 to 1.8 than the predicted ones by ground motion prediction equations (GMPE).

Comparison of our results with GMPEs is very instructive, not only in terms of peak values of motion, but also in terms of the corresponding spatial distribution. In Figure 9, such a comparison is shown with the GMPE proposed by Bindi et al. (2011) based on Italian records (mostly from normal fault earthquakes). The geometric mean of the horizontal components is considered. The GMPE is found to underpredict the simulated values by a factor ranging from 2 to 4 in the vicinity of the source and especially for rock conditions. Also, it is very clear that the adopted distance metric by Bindi et al. (2011), i.e., the Joyner-Boore distance (R_{JB}) from the surface projection of the fault, is not fit to properly describe the spatial distribution of ground motion in near-source conditions. As a matter of fact, by using the R_{JB} metric, all points on the surface fault projection are assigned the same peak value, irrespective of their actual position with respect to the fault rupture. This turns out to play a major role for those faults, either normal or reverse, with medium-to-low dip angles, for which a large surface projection of the fault is expected with a corresponding large variability of ground motion throughout that surface.

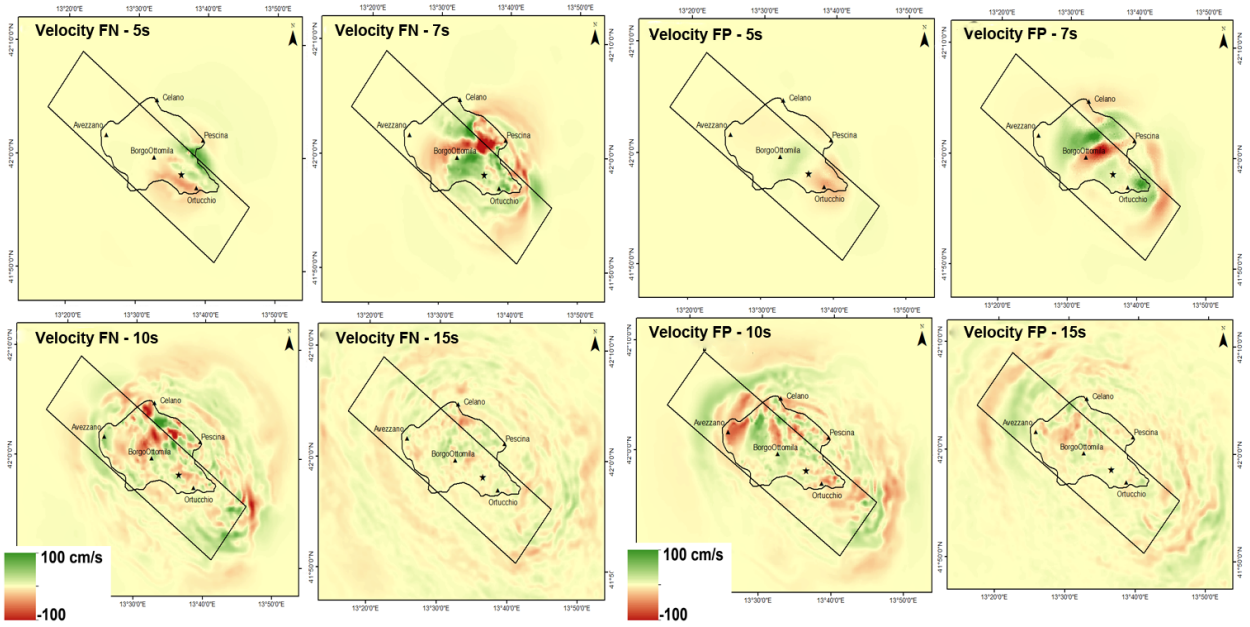

Figure 7. Snapshots of the computed velocity field at different time instants T = 5, 7, 10, 15 s. (Left) Fault Normal (FN) component. (Right) Fault Parallel (FP) component.

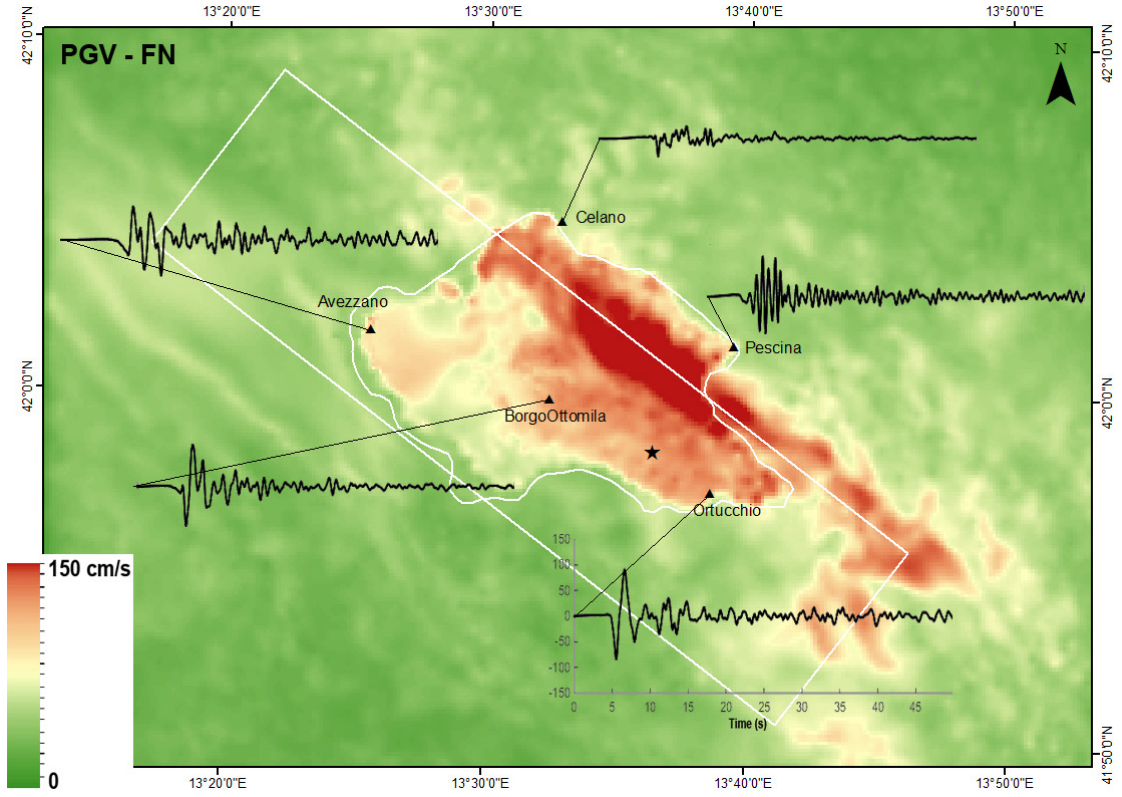

Figure 8. PGV map for the FN component, together with the FN velocity time histories at selected sites (Avezzano, Ortucchio, Pescina, Celano, Borgo Ottomila).

To explore this subject, we have studied the spatial variability of simulated ground motion considering different distance metrics, namely: R_{JB} (Joyner and Boore), R_{EPI} (epicentral), R_{HYP} (hypocentral), R_{RUP} (distance from the fault rupture). In addition to these classical distance metrics, we have also proposed the metric R_{LINE}, that is the distance from the surface fault projection of the segment at the top edge of the fault. The actual position and length of the segment is set by projecting the hypocenter along the edge, and by considering it as the center of a segment of length given by the Wells and Coppersmith (1994) scaling relationships. The resulting segment is shown by a red line on the right hand side map of Figure 9.

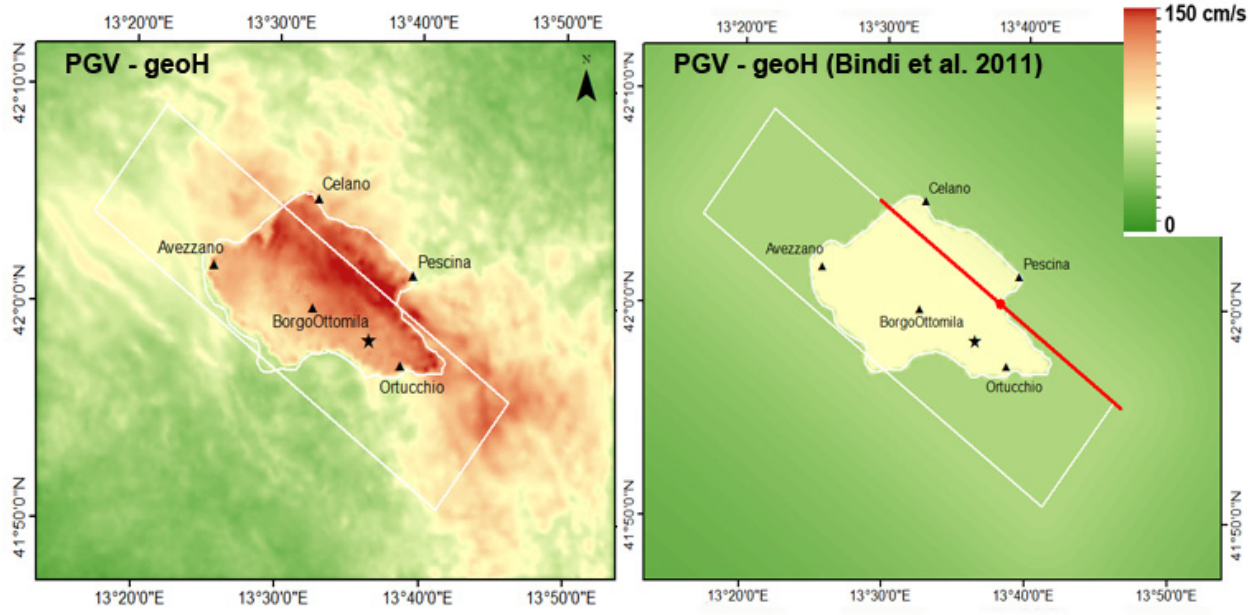

Figure 9. Map of the computed Peak Ground Velocity (PGV). Geometric mean of the horizontal components obtained by SPEED (left) and by GMPE proposed by Bindi et al., (2011), (right).

Considering results in Figure 10, for receivers up to about 40 km distance, the following comments can be made on the application of the different distance metrics:

- R_{EPI}: the scatter of results is very high and, more important, there is no tendency of decreasing amplitude with distance, since the epicenter lies away from the area of largest amplitude;
- R_{HYP}: the limitation is similar as with R_{epi}, with a scatter at short distances exceeding one order of magnitude;
- R_{JB}: a large number of points in this case lies at R_{JB}=0, that was set to a default value of 50 m for representation in a log scale. A similar large scatter as for R_{HYP} is found;
- R_{RUP}: a correct decrease of amplitude with distance can be found, with a lower scatter of results with respect to the previous cases. This may be considered as the best among the "classical" distance metrics typically used in the GMPEs to predict near-source ground motion;
- R_{LINE}: at short distance, the scatter is significantly reduced, while, at large distance, the scatter is similar to the other cases.

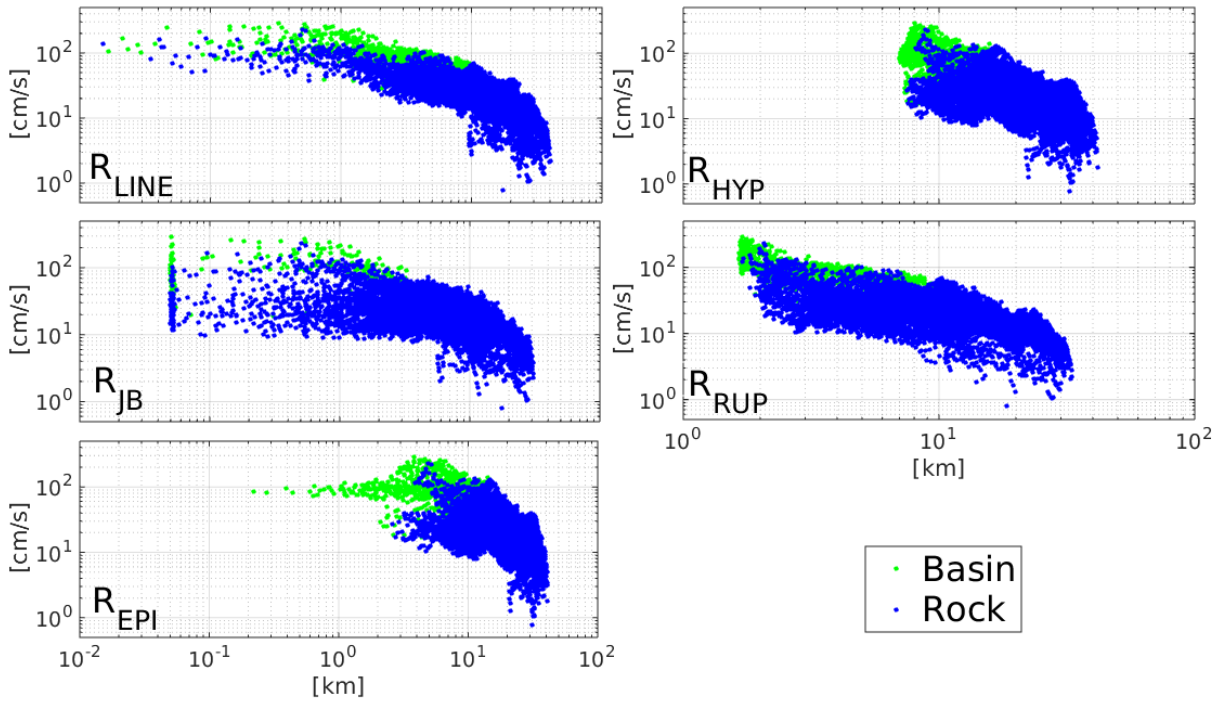

Figure 10. Variability of PGV (FN component) with respect to different distance metrics. Values are expressed in cm/s.

We can conclude that, to improve the accuracy of prediction of ground motion in near-source conditions, especially for large earthquakes, the distance from the fault rupture plane (R_{RUP}) is by far the best metric among the classical ones used for GMPEs. However, the maps of PGV from numerical simulations, as well as the analysis of spatial variability from physics-based simulated ground motions, including also the recent experience with the May 29 2012 Po plain earthquake (Paolucci et al., 2015), suggest that the best performance is obtained through the R_{LINE} distance, that has also the advantage of simplicity of calculation.

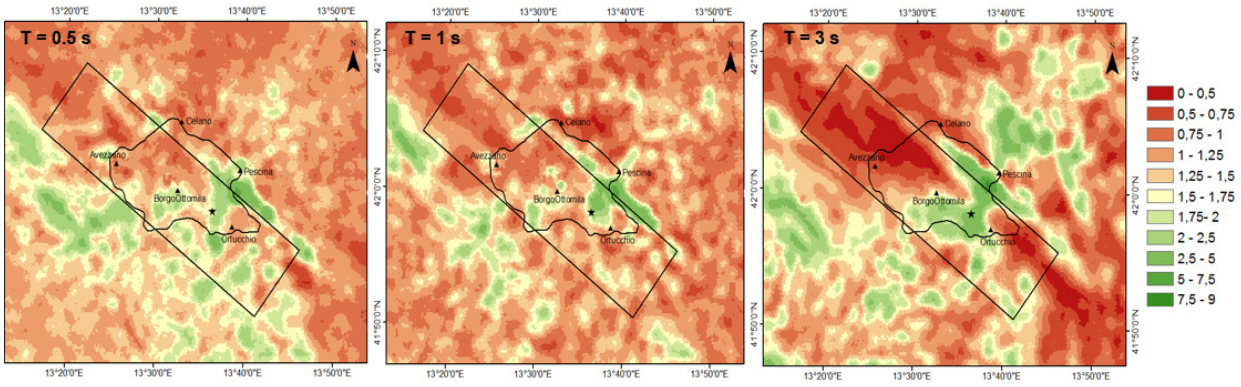

Figure 11: Spatial distribution of the ratio between FN and FP component of acceleration spectrum Sa at 5% damping for T = 0.5 s (left), 1 s (center), 3 s (right).

Finally, we show in Figure 11 the spatial distribution of response spectral ratios (5% damped) of the FN vs FP components of motion, for vibration periods T = 0.5 s, 1 s, 3 s. It can be seen that this ratio is by far larger than 1 in the proximity of the surface fault rupture, as expected for a normal fault. Moving away from the largest asperities of the fault rupture, this ratio decreases to values typically ranging between 1 and 1.5. It is worth noting that, as seen from the right hand side plot on Figure 11, the FP component tend to dominate at long periods (T = 3 s) close to the NW side of the basin, probably due to the dominance of Rayleigh waves propagating in that direction, as noted previously.

Conclusions

This paper has presented results of the 3D physics-based numerical simulations of the 1915 Marsica earthquake, which devastated Avezzano and surrounding villages, causing more than 33,000 fatalities. Good results were obtained, matching reasonably well the geodetic measurements of co-seismic vertical ground displacements, and providing a realistic picture of earthquake ground motion in a condition, quite common in Central Apennines, where there is an interaction of near-source conditions with the complex geology associated to the presence of shallow tectonic basins with relatively soft-soil sediments.

Among the most relevant conclusions of this work we list the following:

- comparison with geodetic measurements is consistent with a M_W 6.7 earthquake magnitude;
- present GMPEs tend to underestimate the earthquake ground motion amplitude in near-source, since they are rather poorly calibrated in such conditions;
- in near-source conditions, a careful choice should be made in terms of distance metric: among the classical metrics, R_{RUP} turns out to be the best one, but the metric R_{LINE}, introduced in this work, provides better performance than R_{RUP};
- as expected for a normal earthquake, the FN component exceeds significantly the FP one in the proximity of the fault, suggesting that in near-source conditions the reference system oriented along the strike of the fault is the best one to make predictions on the largest components of motion;
- the 3D physics-based numerical simulations are capable to provide realistic ground shaking scenarios of past and future earthquakes, and are expected to provide in the future an effective alternative to real records, aiming at calibrating prediction tools of earthquake ground motions.

The study of other features of the simulated ground motions, including the measure of small-scale spatial variability and the impact of the vertical components, is still in progress.

Acknowledgments

This work was stimulated by the invitation received by the first author from Fabrizio Galadini, INGV, to present a lecture at the conference in Avezzano to commemorate the centennial from the earthquake. Fabrizio Galadini and Gianluca Valensise, INGV, provided useful comments and research material that was used to better constrain the numerical model. Funding from the DPC-RELUIS Project RS2, on Numerical simulations and near-source effects, is also gratefully acknowledged.

References

Amoruso A, Crescentini L, Scarpa R. Inversion of source parameters from near and far-field observations: an application to the 1915 Fucino earthquake, Central Apennines, Italy. *Journal of Geophysical Research* 1998; **103**(B12): 29,989-29,999.

Anderson JG, Kawase H, Biasi GP, Brune JN, Aoi S. Ground Motions in the Fukushima Hamadori, Japan, Normal-Faulting Earthquake. *Bulletin of the Seismological Society of America* 2013; **103**: 1935–1951.

Antonietti PF, Mazzieri I, Quarteroni A, Rapetti F. Non-conforming high order approximations of the elastodynamics equation, *Computer Methods in Applied Mechanics and Engineering* 2012; **209-212**(0): 212 – 238.

Butcher JC. *Numerical Methods for Ordinary Differential Equations*, 2nd Edition ,Wiley, 2008.

Basili A and Valensise G. Contributo alla caratterizzazione della sismicità dell'area marsicano-fucense. in Proc. II Workshop on "*Aree Sismogenetiche e Rischio Sismico in Italia*", E. Boschi and M. Dragoni (eds) Erice 1986, 1991; 197-214.

Berardi R, Mendez A, Mucciarelli M, Pacor F, Longhi G, Petrungaro C. On the modelling of strong motion parameters an correlation with historical macroseismic data: an application to the 1915 Avezzano earthquake. *Annali di Geofisica* 1995; **38**: 851-866.

Bindi D, Pacor F, Luzi L, Puglia R, Massa M, Ameri G, Paolucci R. Ground motion prediction equations derived from the Italian strong motion database. *Bull Earthquake Eng.* 2011; **9**:1899–1920.

Cara F, Di Giulio G, Cavinato GP, Famiani, Milana G. Seismic characterization and monitoring of Fucino Basin (Central Italy). *Bull. Earthquake Eng* 2011; **9**:1961-1985.

Cavinato GP, De Celles PG. Extensional basins in the tectonically bimodal central Apennines fold-thrust belt, Italy: response to corner flow above a subducting slab in retrograde motion. *Geology* 1999; **27** (10): 955-958.

Cavinato GP, Carusi C, Dall'Asta M, Miccadei E, Piacentini T. Sedimentary and tectonic evolution of Plio-Pleistocene alluvial and lacustrine deposits of Fucino basin (Central Italy). *Sedimentary Geology* 2002; **148**: 29-59.

Faccioli E, Maggio F, Paolucci R, Quarteroni A, 1997. 2D and 3D elastic wave propagation by a pseudo-spectral domain decomposition method. *Journal of Seismology* 1997; **1**(3): 237–251.

Favali P and Frugoni F. Revisione critica dei parametri fisici del terremoto. In: "*13 gennaio 1915. Il terremoto nella Marsica"* a cura di S. Castenetto e F. Galadini 1999; 273-282.

Guidoboni E, Ferrari G, Mariotti D, Comastri A, Tarabusi G, Valensise G. CFTI4Med, Catalogue of Strong Earthquakes in Italy (461 B.C.-1997) and Mediterranean Area (760 B.C.-1500). *INGV-SGA 2007*. Available from http://storing.ingv.it/cfti4med/ (Last access: May 2015).

Galli P, Messina P, Giaccio B, Peronace E, Quadrio B. Early Pleistocene to late Holocene activity of the Magnola fault (Fucino fault system, central Italy). *Bollettino di Geofisica Teorica ed Applicata* 2012; **53**: 435-458.

Galadini F and Galli P. The Holocene paleoearthquakes on the 1915 Avezzano earthquake faults (central Italy): Implications for active tectonics in Central Apennines. *Tectonophys* 1999; **308**: 143-170.

Galadini F, Galli P, Giraudi C. Geological investigations of Italian earthquakes: new paleoseismological data from the Fucino plain (Central Italy), *Journal of Geodynamics* 1997; **24**:87-103.

Giraudi C. Evoluzione geologica tardo pleistocenica ed olocenica della Piana del Fucino e dei versanti adiacenti: analisi di nuovi dati stratigrafi ci e radiometrici e ricostruzione delle variazioni ambientali. In *13 Gennaio 1915. Il terremoto della Marsica* (a cura di Castenetto S. e Galadini F.). C.N.R., Serv. Sis. Naz., Ist. Poligr. Stat. Roma 1999; 183-197.

Hardin BO and Drnevich VP. Shear modulus and damping in soils: Design equations and curves. *Journal of Soil Mechanics and Foundation Division* 1972; **98**:667-692

Komatitsch D and Tromp J. Introduction to the spectral-element method for 3-D seismic wave propagation. *Geophysical Journal International* 1999; **139**(3): 806–822.

Locati M, Camassi R, Stucchi M. DBMI11, la versione 2011 del Database Macrosismico Italiano 2011. Milano, Bologna, http://emidius.mi.ingv.it/DBMI11. DOI: 10.6092/INGV.IT-DBMI11.

Loperfido A. Indagini astronomico-geodetiche relative al fenomeno sismico della Marsica, 95 pp., Atti Minist. Lavori Pubblici, Florence, Italy, 1919.

Mazzieri I, Stupazzini M, Guidotti R, Smerzini C. SPEED: SPectral Elements in Elastodynamics with Discontinuous Galerkin: a non-conforming approach for 3D multi-scale problems. *International Journal for Numerical Methods in Engineering* 2013; **95**(12): 991–1010.

Moczo P, Kristek J, Galis M. *The Finite-Difference Modelling of Earthquake Motions: Waves and Ruptures*. Cambridge University Press 2014.

Oddone E.Gli elementi fisici del grande terremoto marsicano fucense del 13 Gennaio 1915. *Boll. Soc. Sismol.* It. 1915; **29**: 71-215.

Pane V and Burghignoli A. *Determinazione in laboratorio delle caratteristiche dinamiche dell'argilla del Fucino*. CNR 1988.

Paolucci R, Mazzieri I, Smerzini C, Stupazzini M. Physics-based earthquake ground shaking scenarios in large urban areas, in Perspectives on European Earthquake Engineering and Seismology, Geotechnical, *Geological and Earthquake Engineering* ed. Ansal, A., Springer 2014; **34**: 10.

Paolucci R, Mazzieri I, Smerzini C. Anatomy of strong ground motion: near-source records and 3D physics-based numerical simulations of the Mw 6.0 May 29 2012 Po Plain earthquake, Italy. Submitted for publication to Geophysical Journal International, 2015.

Patera AT. A spectral element method for fluid dynamics: laminar flow in a channel expansion. *Journal of Computational Physics* 1984; **54**: 468–488.

Seriani G, Priolo E, Pregarz A. Modelling waves in anisotropic media by a spectral element method. Proceedings of the *third international conference on mathematical and numerical aspects of wave propagation* 1995; 289–298.

Smerzini C, Villani M. Broadband Numerical Simulations in Complex Near-Field Geological Configurations: The Case of the 2009 Mw 6.3 L'Aquila Earthquake. *Bulletin of the Seismological Society of America* 2012; **102**: 2436–2451.

Stacey R. Improved transparent boundary formulations for the elastic-wave equation, *Bulletin of the Seismological Society of America*, 1988; **78**(6): 2089–2097.

Stupazzini M, Paolucci R, Igel H. Near-fault earthquake ground-motion simulation in the Grenoble valley by a high-performance spectral element code, *Bulletin of the Seismological Society of America* 2009; **99**(1): 286–301.

Ward SN, Valensise G. Fault parameters and slip distribution of the 1915 Avezzano, Italy, earthquake derived from geodetic observations. *Bulletin of the Seismological Society of America* 1989; **79**: 690–710.

Wells DL, Coppersmith KJ. New Empirical Relationships among Magnitude, Rupture Length, Rupture Width, Rupture Area, and Surface Displacement. Bulletin of the Seismological Society of America 1994; **84**: 974–1002.

Working Group MS–AQ. *Microzonazione sismica per la ricostruzione dell'area aquilana Regione Abruzzo* – Dipartimento della Protezione Civile, L'Aquila, 3 and Cd-rom 2010.